



Effective adsorption of cationic dye from aqueous solution using low-cost corncob in batch and column studies

Syed Mubashar Hussain Gardazi^a, Tayyab Ashfaq Butt^b, Naim Rashid^c,
Arshid Pervez^a, Qaisar Mahmood^a, Mohammad Maroof Shah^a, Muhammad Bilal^{a,*}

^aDepartment of Environmental Science, COMSATS Institute of Information Technology, University Road, Tobe Camp Postal Code 22060, KPK, Abbottabad, Pakistan, Tel. +92 992 383591 6, ext. 308; Fax: +92 992 383441; email: smgardazi@ciit.net.pk (S.M. Hussain Gardazi), Tel. +92 992 383591 6, ext. 320; Fax: +92 992 383441; email: pervez@ciit.net.pk (A. Pervez), Tel. +92 992 383591 6, ext. 372; Fax: +92 992 383441; email: drqaisar@ciit.net.pk (Q. Mahmood), Tel. +92 992 383591 6; Fax: +92 992 383441; email: mmshah@ciit.net.pk (M. Maroof Shah), Tel. +92 992 383591 6, ext. 308; Fax: +92 992 383441; email: mbilal@ciit.net.pk (M. Bilal)

^bDepartment of Civil Engineering, University of Hail, Hail, Kingdom of Saudi Arabia, Tel. +966 55 180 7802; Fax: +966 653 10500; email: ta.butt@uoh.edu.sa

^cDepartment of Chemical Engineering, COMSATS Institute of Information Technology, Defence Road, Lahore, Pakistan, Tel. +92 42 111 001 007, ext. 124; Fax: +92 42 99203100; email: naimkanwar@yahoo.com

Received 17 December 2015; Accepted 4 May 2016

ABSTRACT

Dye effluents and their degradation products disrupt the aquatic ecosystem functioning. Corncob was used as a low-cost biosorbent for decolorization of methylene blue (MB) dye. Batch and fixed-bed column adsorption were performed by varying temperature, pH, initial dye concentration, adsorbent dose, particle size, and bed height, flow rate and inlet dye concentration, respectively. High MB adsorption capacities of corncob were attained at pH 9, i.e. 45.86 mg g⁻¹, 91.7%. Equilibrium data was best described by Langmuir II ($R^2 = 0.999$) followed by Freundlich ($R^2 = 0.994$) and Halsey ($R^2 = 0.994$) isotherm models, which indicates the favorable adsorption of MB dye onto corncob adsorbent. Moreover, chemisorption nature of corncob was confirmed through Dubinin–Radushkevich ($E = 16.01$ kJ mol⁻¹) and the best fit of pseudo-second-order kinetic model. Thermodynamic studies revealed spontaneous ($\Delta G < 0$) and endothermic ($\Delta H > 0$) nature of reaction with increased randomness ($\Delta S > 0$) at the solid–liquid interface. The breakthrough curves were predicted using Thomas and BDST models. BDST reflected that 2.26 min were required to exhaust 1 cm of the fixed-bed column. MB dye-loaded corncob adsorbent could be regenerated (80%) and reused using 0.1 M acetic acid.

Keywords: Corncob biosorbent; Methylene blue dye; Isotherm; Thermodynamic; Thomas and BDST models

*Corresponding author.

1. Introduction

Dyes are being used in various industries like textile, leather, cosmetics, and paper. The wastewater from such industries is produced in operational steps of color washing, whitening, dyeing, and printing. In developing countries like Pakistan, the waste effluents from these industries enter the freshwater ecosystem without treatment and ultimately disrupt the ecosystem functioning [1]. These dyes are highly carcinogenic, and therefore, pose a serious threat to human health and aquatic life. So, it is imperative to eliminate the risk of trapping the colors in wastewater and environmental hazards.

Various techniques, including chemical oxidation, membrane filtration, precipitation, ion exchange, biosorption, and adsorption, are adopted to remove the hazardous metals and dyes from the aqueous solutions [2–6]. Among them, biosorption has been suggested as a potential alternative for detoxification and recovery of toxic dyes from wastewater because of the low operational cost, maintenance, and simplicity [7–10]. A number of biosorbents such as rice husk, peat, de oiled soya, peat resin, hen feather, modified *hibiscus* fiber, and ash have been used for the dyes removal [8,11–16]. The activated carbon has been prepared from waste biomasses by physical and chemical modifications, which increases the cost and energy input. Different untreated waste from agriculture and forest sectors can be a subject for intensive research, especially for dyes and metals removal [17,18]. Among the agricultural biomasses, maize is the second largest grown crop in Khyber Pakhtunkhwa, province of Pakistan, whereas third cereal crop in the country after wheat and rice. This province contributes almost 68% of total production of the country, i.e. 3.5 million metric tonnes, and total area under maize cultivation is 57% of the country, i.e. 1 million hectare [19]. Besides, its beneficial use as fodder crop (leaves and stalks) and grains, a large volume of waste, containing corncob (CC), is disposed off. Therefore, this waste can be used as a cheap adsorbent for the pollutants' removal from wastewaters in the Pakistan scenario. The dye or metal sorption efficiency of various waste biomasses or their activated forms has been investigated often through batch experiments [20]. However, the continuous adsorption in fixed-bed column is imperative from wastewater treatment design point of view at industrial scale. Therefore, the batch and fixed-bed column studies are required simultaneously for a comprehensive investigation of sorption efficiency of any unmodified or activated form of adsorbent. Although spent corncob has been used as an adsorbent previously [21], however it has not been

used for removal of methylene blue (MB) dye directly. Furthermore, both the batch and column studies were conducted to explain the mechanism of MB adsorption. Additionally desorption studies were also conducted in the end to look at the possible adsorbent regeneration for field application. To date very few studies have been conducted incorporating all of these aspects into one study. The effects of various parameters for both experimental modes were explored and optimized for maximum adsorption potential of corncob for a targeted contaminant. The fixed-bed column is simple to operate, and can be scaled-up from a laboratory process [22].

The selected dye MB is commonly used in coloring paper, cotton, and wool industries. However, MB is considered to be toxic dye for human and aquatic life. The ingestion of MB dye by human resulted in respiratory illness, diarrhea, nausea, and eye burns [23,24]. In the current study, a low-cost and abundantly available corncob (CC) was explored for MB, cationic dye, removal in batch and column mode. The effect of various parameters such as contact time, initial dye concentration, temperature, pH, particle size, and adsorbent dose was optimized in batch experiments. The effect of various flow rates, bed heights, and initial dye concentrations on the MB adsorption of CC were also optimized for fixed-bed column experiments. The mechanisms and adsorptive nature of the CC, during the batch process for MB dye, were elucidated using isotherms, kinetic model, and thermodynamic studies. The column adsorption data was studied by Thomas and BDST models.

2. Experimental

2.1. Materials and instrumentation used

The cationic dye i.e. methylene blue C.I. 52015 (Fig. 1), was purchased from Merck Germany. Stock solution of dye was prepared by dissolving 1 g of dye in 1,000 mL of deionized water, and the subsequent dilutions were done to prepare the working solutions

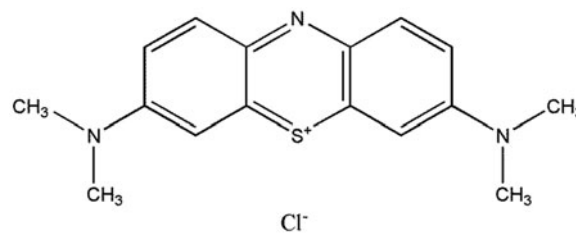


Fig. 1. Structure of MB dye.

of required dye concentrations. Grinding mill was used to obtain the required particle size. The solution pH was adjusted with 0.1 M HCl and 0.1 M NaOH and it was measured by a digital pH meter (Model: PHS-25CW, Shanghai). SEM was performed on Hitachi S-3000 N, Japan. Double beam UV spectrophotometer (PG T80+, UK) was used to measure the residual MB dye at λ_{\max} 668 nm. Functional group surface chemistry of the adsorbent, before and after MB dye adsorption, was explored using KBr disk by IRPrestige-21 Shimadzu Japan and FTIR spectra were recorded in the region of 4,000–600 cm^{-1} . Orbital shaking incubator (Wise cube 20, Korea) having an automated fuzzy control system was used to shake the dye and adsorbent mixture under the controlled temperature and required agitation (rpm) conditions.

2.2. Preparation of adsorbent

Corncocks (CC) were collected locally from Abbotabad, Khyber Pakhtunkhwa (KPK) province of Pakistan. After the removal of grains, the waste corncocks were used as adsorbent. It was cut into pieces, washed with deionized water. After drying, these cobs were grounded in grinding mill, and sieved to obtain the required particle sizes (105–400 μm).

2.3. Batch experiments

These experiments were performed in a conical flask (100 mL volume) having 50 mL solution at constant conditions of temperature (303 K), shaking speed (220 rpm), working solution pH (6.8), adsorbent dose (0.05 g), and initial MB dye concentration of 50 mg L^{-1} . After shaking for a particular time, the solution mixture was centrifuged at 4,000 rpm for 10 min, and the supernatant was filtered through 0.45 μm filter paper. The equilibrium distribution of MB dye between the adsorbent and aqueous solution was recorded for 24 h. The effect of the individual reaction and environmental parameter on the removal capacity of CC were examined, while keeping the rest of aforesaid conditions constant. These parameters include pH (3–9), temperature (303–323 K), initial adsorbate concentration (30–300 mg L^{-1}), particle size (105–400 μm), and the amount of adsorbent (0.05–5 g). The adsorption capacity (q_e , mg g^{-1}) of the CC for MB dye, and its sorption efficiency (S %) were calculated using Eqs. (1) and (2), respectively:

$$q_e = \left(\frac{C_0 - C_f}{m} \right) V \quad (1)$$

$$S(\%) = \left(\frac{C_0 - C_f}{C_0} \right) \times 100 \quad (2)$$

where C_0 and C_f were the initial and final solution concentrations (mg L^{-1}) of MB dye, respectively. m and V are the mass of the studied adsorbent (g) and volume of the solution (L), respectively.

2.4. Column experiments

These experiments were conducted in cylindrical glass columns (2.5 cm internal diameter) at room temperature. At the bottom of the column, glass wool was packed followed by 3 mm glass beads. The adsorbent dose of 7.5 g was placed into the column, yielding bed height of 5 cm. Glass beads were also placed at the top of the column for even distribution of the dye solution. Solutions with the known MB dye concentrations were pumped downward through the column bed. Samples were collected at the column outlet at different time intervals and were analyzed for the residual MB dye concentration. The effect of the inlet concentrations of MB dye were varied from 50 to 300 mg L^{-1} , the flow rates of dye solutions were varied from 5 to 10 mL min^{-1} , and similarly the range of bed height was 5–10 cm at a fixed inlet concentration of 50 mg L^{-1} . The effect of the individual column parameter on the removal capacity of CC was examined while keeping the rest of aforesaid conditions constant. These parameters include the inlet concentrations of MB dye (50–300 mg L^{-1}), the flow rates of dye solutions were varied from 5 to 10 mL min^{-1} , and similarly the range of bed height was 5–10 cm.

2.5. Desorption studies

Different acids (CH_3COOH , HCl, H_2SO_4 , HNO_3) of 0.1 M concentrations and solvents (acetone, ethanol, methanol) were used as eluents in desorption studies. The CC 0.05 g was saturated with 50 mL solution having 50 mg L^{-1} of initial MB dye concentration. Shaking was carried out at 220 rpm for 200 min in a temperature controlled orbital shaker. At equilibrium, the adsorbent was filtered and washed with deionized water to remove MB traces. The adsorbent was treated with 50 mL of aforesaid eluents. The flasks were again shaken at 220 rpm for 120 min and desorbed concentration of MB in the eluent was determined. The desorption (%) of MB dye was calculated using Eq. (3):

$$\% \text{ Desorption} = \left(\frac{C_d \cdot V_d}{q_e \cdot W} \right) \times 100 \quad (3)$$

where C_d is the concentration of desorbed adsorbate (mg L^{-1}), V_d the volume of desorption solution (L), W is the mass of the pre-adsorbed adsorbent (g), and q_e is the amount of adsorbate adsorbed per unit of the adsorbent (mg g^{-1}).

2.6. Isotherm, kinetics, and thermodynamics studies

Different adsorption isotherm and kinetic models were applied on the MB adsorption data of CC by simulating the variable initial dye concentrations of 30–300 mg L^{-1} . Whereas the reaction parameters, i.e. temperature (303 K), pH (6.8), shaking speed (220 rpm), contact time (200 min), and adsorbent dose (0.05 g) were kept constant. Among the isotherm models, Langmuir, Temkin, Dubinin–Radushkevich (D–R), Freundlich, Halsey, and Brunauer–Emmett–Teller (BET), were applied. Mechanism of MB adsorption onto the CC was elucidated using the pseudo-first-order and pseudo-second-order kinetic models. The corresponding constants and correlations of the model plots were calculated. Moreover, thermal, spontaneity, and randomness of the MB adsorption were investigated at the solid–liquid interface.

2.7. Surface characterization of the adsorbent

SEM analyses were conducted to study the morphology of adsorbent after MB dye adsorption. Samples were mounted on brass stubs using double-sided adhesive tape. SEM images were taken with scanning electron microscope (HITACHI S-3000 N, JAPAN) at magnifications of 100 \times , 500 \times , and 1,000 \times . These images were collected at 5 kV acceleration voltage, and the working distance of 25 mm was maintained. EDX spectrum was recorded to reveal the variations in elemental composition of CC before and after MB dye adsorption. Changes in the functional group surface chemistry of CC after MB dye adsorption were detected using FTIR analysis.

3. Results and discussion

3.1. SEM and EDX analyses

The morphological analysis of CC was investigated through SEM images (Fig. 2). These images clearly reflected the porous structure of CC adsorbent, where the primary and secondary pores were identified, supporting the adsorption phenomenon. The SEM image at 1,000 \times showed the binding of dye molecules on the pore surface. However, the adsorbent surface can accommodate more adsorbate in its primary and secondary pores even after removal of MB dye, i.e.

96 mg g^{-1} at initial dye concentration of 150 mg L^{-1} . EDX analysis showed the quantitative presence of various elementals [weight (%)] in CC adsorbent, representing that CC was composed mainly of C (52.70.95%), O (46.92%), K (0.38%) before MB dye adsorption. After treatment, the MB dye was confirmed by the evidence of the change in elemental composition C (52.89%), N (4.27%), O (42.12%), Cl (0.35%), and S (0.37%) of adsorbent, especially, the Cl, S, and N which are present in the MB structure and composition (Fig. 2).

3.2. FTIR analysis

Chemical composition of corncob and functional groups present on its surface were determined by FTIR analysis. Chemical composition is of vital importance to understand the adsorption phenomena, particularly when it is chemisorption. Fig. 3 presents the FTIR spectrum of CC, before and after adsorption of MB dye loading and in the inset difference in the peaks can be seen. The characteristic peak due to C–N (aliphatic amines) stretching bond in CC appeared at 1,035 which also appeared in the sample after adsorption. The smaller peak appeared at 2,929 cm^{-1} is attributed to the C–C stretching bond in organic adsorbent. The peak at 3,360 cm^{-1} is ascribed to O–H stretching, and it indicates the presence of alcoholic and hydrogen bonded water in the cell wall of CC. The presence C–O–C (ethers) appears at 1,242 cm^{-1} . The distinctive peak appears at 885 cm^{-1} , which is the addition of the C–H (aromatics) after the adsorption of MB dye. Similarly, the appearance of new peaks at 1,330 and 1,386 cm^{-1} are associated with the C–N stretch (aromatic amines) and C–H bending (CH_2 and CH_3), respectively, after attachment of the dye components onto the adsorbent surface. The additional peak at 1,598 is attributed to vibration of carbon to carbon stretch (C–C), which indicates the chemisorbed MB functional groups.

3.3. Batch adsorption

3.3.1. Effect of contact time

The effect of contact time was examined and equilibrium time was determined, thus evaluating the shortest time required for MB dye adsorption by CC (Fig. 4). The data revealed that contact of 200 min is sufficient to achieve the equilibrium adsorption, i.e. (41.73 mg g^{-1} , 82%) using MB dye concentration of 50 mg L^{-1} . Further increase in contact time did not significantly change the adsorption even when the batch experiment was run for 480 min (Fig. 4). There

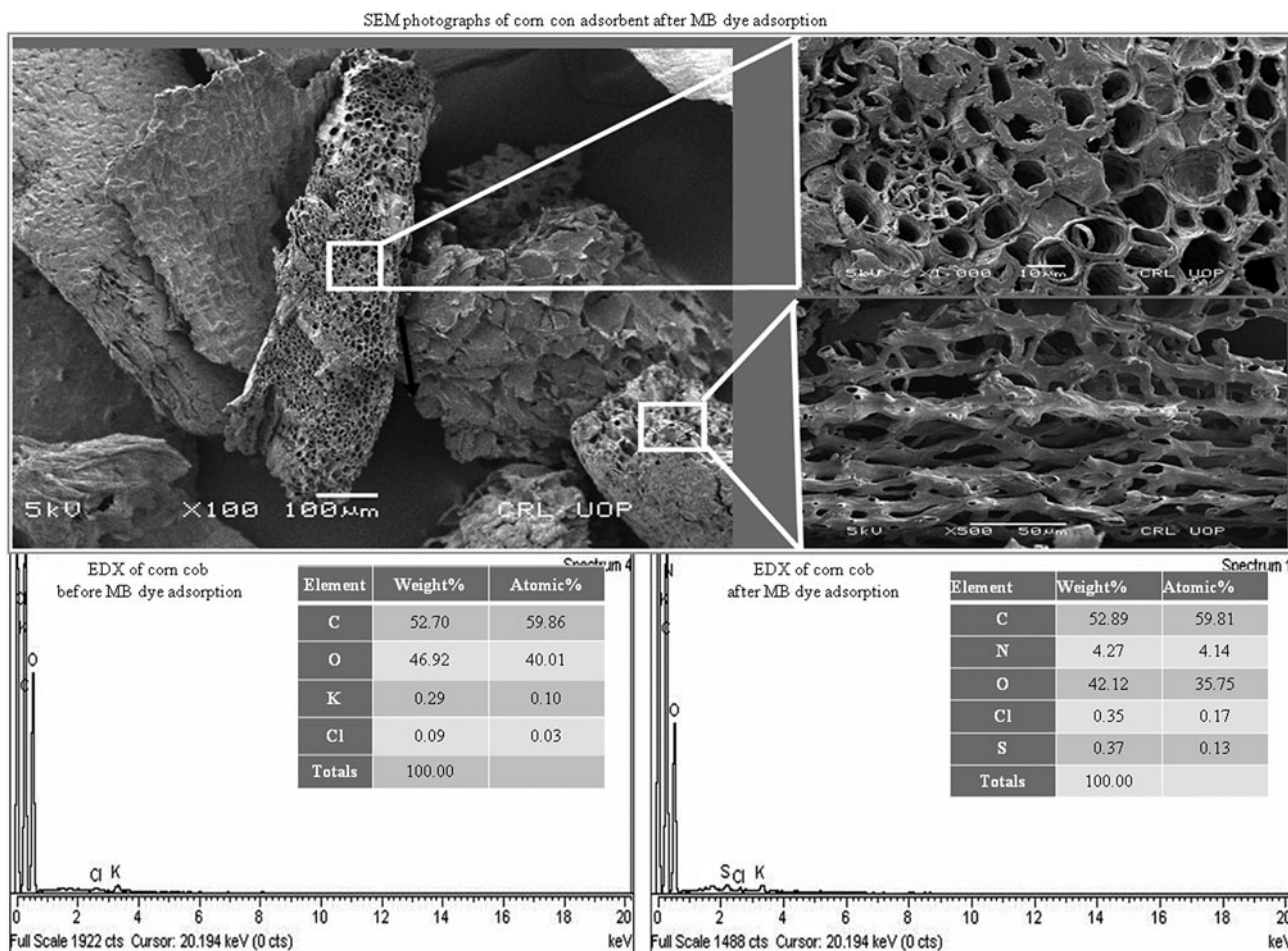


Fig. 2. SEM and EDX analyses CC biosorbent.

can be multiple reasons for the longer equilibrium time: (i) dye molecule cross the external boundary layer toward the solid surface of adsorbent; (ii) adsorbate diffusion from particle surface toward the active site within the pore filled liquid and then migration along the solid surface of pore; (iii) dye molecule adsorption on the active sites of pores' interior surface; (iv) after adsorption, dye molecule can migrate on the surface of pore through surface diffusion. During the biosorption process, initially a rapid dye uptake was observed, followed by a slower dye removal. Abundant availability of the active sites and the resistance of aggregated dye molecules on the adsorbent surface could be reasons of the rapid and slower phases of MB dye adsorption [25–27].

3.3.2. Effect of adsorbent particle size

The particle size of an adsorbent could be one of the important factors affecting its sorption efficiency

for a target contaminant. Fig. 4 revealed significant ($p = 0.01$) decrease in MB adsorption ($47\text{--}41\text{ mg g}^{-1}$) with increasing the particle size of the adsorbent, i.e. $105\text{--}400\text{ }\mu\text{m}$. This is due to the increase in total surface area for smaller size particles, which provides better accessibility of MB dye molecules into secondary and tertiary pores of the adsorbent. Moreover, higher number of active pores have been observed in small particle size of adsorbent than large particles, which increase the dye uptake capacity [28]. Similarly, the diffusion resistance to mass transport from larger particles is high, and most of the internal surface of the particle may not be utilized for adsorption. Consequently, the amount of adsorbed MB dye decreases.

3.3.3. Effect of adsorbent dose

The sorption efficiency of CC increased from 46 to 99% upon the incremental increase in adsorbent dose from 0.25 to 5.0 g L^{-1} , respectively (Fig. 4). This is due

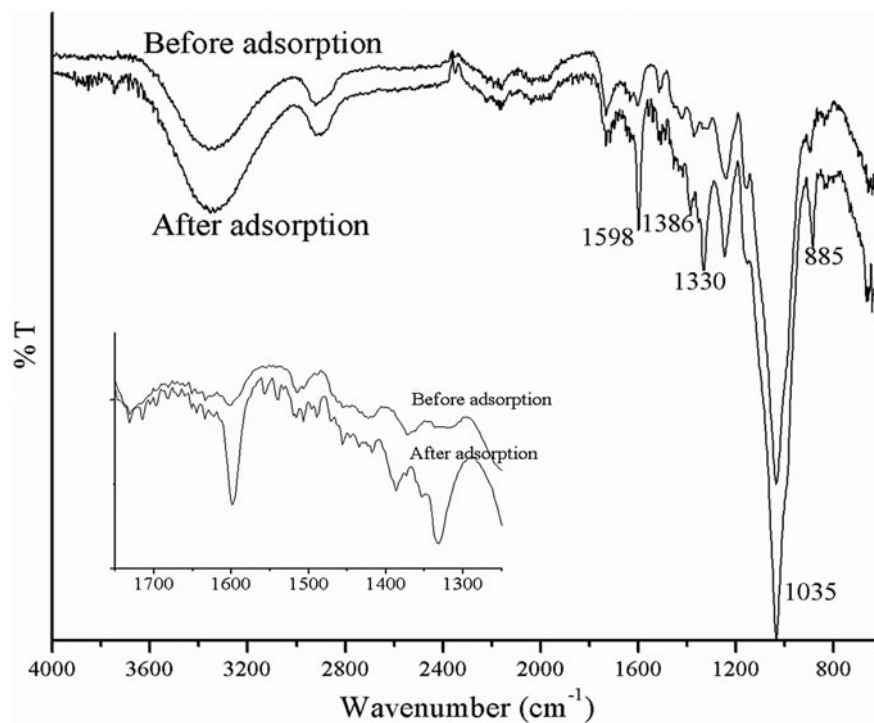


Fig. 3. FTIR analysis of CC biosorbent.

to the availability of more active sites. However, the adsorption of MB dye per unit weight of adsorbent decreased significantly ($p = 0.01$) from 93.15 to 9.98 mg g^{-1} with increasing CC dose from 0.25 to 5.0 g L^{-1} , respectively. This can be attributed to partial overlapping or aggregation at a higher adsorbent dose, which results in a decrease in total surface area and active sorption sites [29,30]. Moreover, data did not reflect any significant MB dye removal (16.45 – 9.98 mg g^{-1}) at CC dose from 3.0 to 5.0 g L^{-1} , which could be ascribed to the higher number of unsaturated active binding sites during the biosorption process [31,32]. Therefore, 1 g of adsorbent was enough to remove the MB dye in the present investigation.

3.3.4. Effect of pH

Solution pH is an important controlling parameter for dyes biosorption. MB is a cationic dye, which exists in the aqueous solution in the form of positively charged ions. Being cationic species, the degree of its adsorption onto the CC surface is primarily influenced by the surface charge on the adsorbent, which in turn is effected by the solution pH. MB adsorption onto CC surface was significantly lower (13.75 mg g^{-1}) at pH 3

than 45.867 mg g^{-1} at pH 9 (Fig. 4). It can be ascribed to the excess H^+ ions, which can compete for active adsorption sites with the cation groups on MB dye molecules, and repulsive force is developed between the positively charged adsorbent and cation dye. Besides this, hydrogen bonding also decreased between the adsorbent and dye molecule. Moreover, at a high solution pH, the positive charges decrease at the solid–liquid interface and the adsorbent surface becomes negatively charged. This results in high MB dye removal.

3.3.5. Effect of dye concentration

The initial concentration of dye provides an important driving force to overcome the mass transfer resistance of dye molecules between the aqueous and solid phases. Data revealed that MB adsorption capacity of CC increased from 18.73 to $117.108 \text{ mg g}^{-1}$ with increasing initial dye concentration from 30 to 300 mg L^{-1} , respectively (Fig. 5). This is probably due to a high-mass transfer driving force. However, the percentage removal of dye decreased from 83.45 to 39.03% with the given increase of initial dye concentration, which was expected due to the saturation of active binding sites of CC.

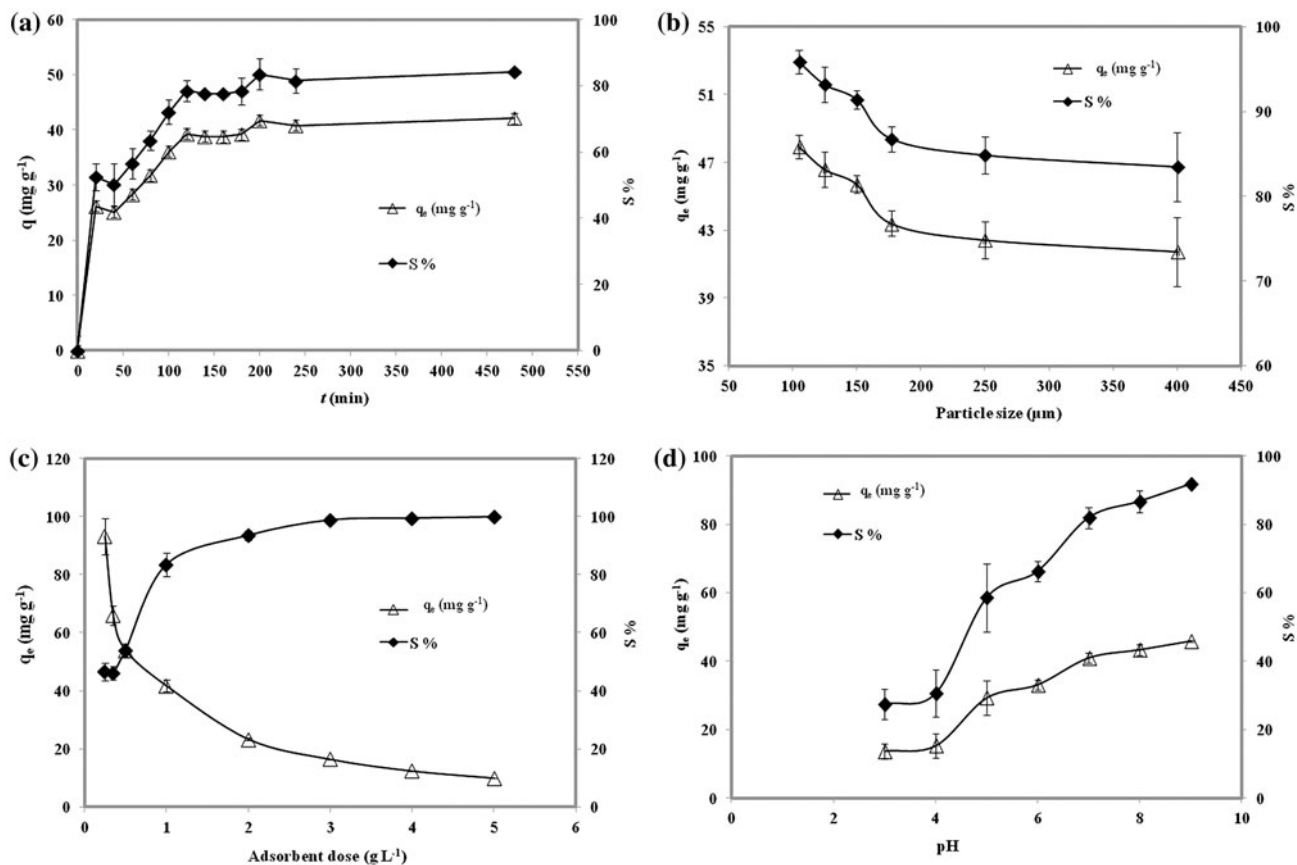


Fig. 4. Effect of contact time (a) particle size (b), adsorbent dose (c), and pH (d) on MB adsorption capacity of CC.

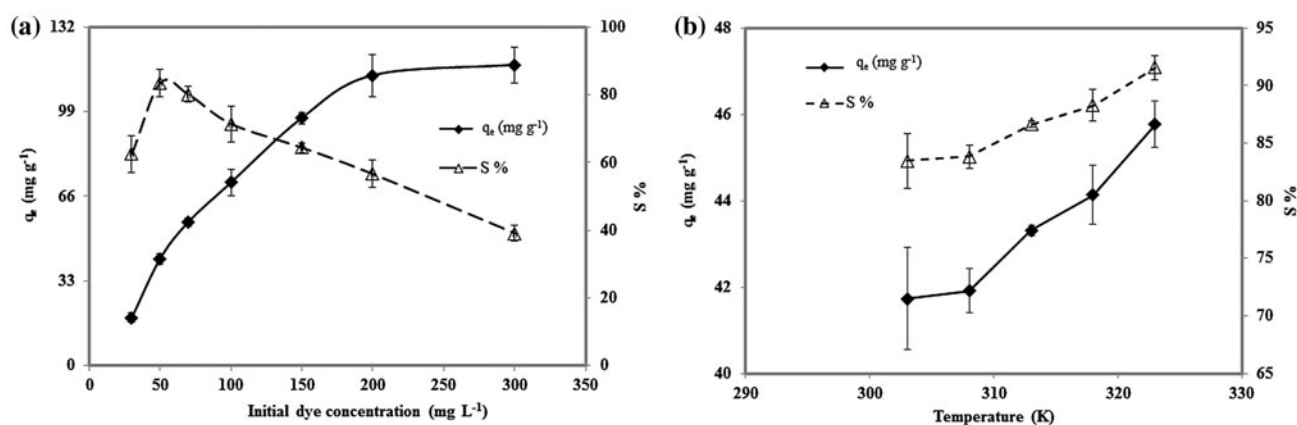


Fig. 5. Effect of initial dye concentration (a) and temperature (b) on adsorption capacity of CC at equilibrium time.

3.3.6. Effect of temperature

Effect of temperature on MB adsorption is presented in Fig. 5. The adsorption capacity and percentage removal increased slightly with increasing temperature. Results show that the MB adsorption on

CC is an endothermic process. The increase in adsorption capacity (41.72–45.76 mg g⁻¹) and percentage removal (83.45–91.53%) could be associated to increase in the mobility of the MB dye molecules with increasing temperature (303–323 K). Moreover, large number

of dye molecules may also acquire sufficient energy to undergo an interaction with active sites on the adsorbent surface. Furthermore, the temperature rise produces the swelling effects on the internal structure of the adsorbent and enlargement of pore size, which facilitate the further penetration of dye molecules. Similar results have been reported by adsorption of MB on green pea peels [33,34].

3.4. Adsorption isotherms

Isotherm studies are essential to find a correlation between the adsorption capacity (q_e , mg g⁻¹) and the residual concentration (C_e , mg L⁻¹) of adsorbate in the aqueous phase [35,36]. Various isotherm models, i.e. Langmuir [37], Freundlich [38], Dubinin–Radushkevich (D–R) [39], Temkin [40], were used to elucidate the nature and optimization of the studied adsorption system (Table 1).

3.4.1. Langmuir isotherm

This model assumes the presence of active sites on the adsorbent surface and no significant interactions

Table 1
Constants of various isotherm models

| Isotherms | Parameter | Unit | Value |
|----------------------|-----------|-------------------------------------|--------|
| Langmuir II | q_{exp} | (mg g ⁻¹) | 117 |
| | q_{max} | (mg g ⁻¹) | 129.87 |
| | K_{ads} | (L mg ⁻¹) | 19.29 |
| | R^2 | | 0.999 |
| Langmuir I | q_{max} | (mg g ⁻¹) | 129.87 |
| | K_{ads} | (L mg ⁻¹) | 0.056 |
| | R^2 | | 0.9979 |
| Freundlich | K_f | (L g ⁻¹) | 17.77 |
| | $1/n$ | | 0.4191 |
| | n | | 2.39 |
| | R^2 | | 0.9935 |
| Halsey | q_{cal} | (mg g ⁻¹) | 115.41 |
| | n_H | | 2.39 |
| | K | | 959.2 |
| | R^2 | | 0.9935 |
| Temkin | K_T | (L mg ⁻¹) | 2.23 |
| | b_T | (kJ mol ⁻¹) | 83.53 |
| | R^2 | | 0.9871 |
| | | | |
| Dubinin–Radushkevich | q_{DR} | (mol g ⁻¹) | 122.13 |
| | B | (mol g ⁻¹) ² | 0.002 |
| | E | kJ mol ⁻¹ | 16.01 |
| | R^2 | | 0.9815 |

between adsorbed species. The Langmuir isotherm equations applied are as follows:

$$\text{Type I } \frac{1}{q_e} = \frac{1}{K_L \cdot q_{max} C_e} + \frac{1}{q_{max}} \quad (4)$$

$$\text{Type II } \frac{C_e}{q_e} = \frac{1}{K_L \cdot q_{max}} + \frac{C_e}{q_{max}} \quad (5)$$

where q_e is the amount of dye adsorbed on CC (mg g⁻¹) at equilibrium time, C_e is the equilibrium dye concentration (mg L⁻¹), q_{max} is the maximum adsorption capacity describing complete monolayer (mg g⁻¹), and K_L is Langmuir constant related to free energy of adsorption.

Among the studied linear models of Langmuir, (Fig. 6), type II reflected the best fit (R^2 , 0.999) to the equilibrium data followed by type I (R^2 , 0.9979). The values of various constants of the model are presented in Table 1. The higher correlation coefficient and closeness of q_{exp} and q_e confirmed the applicability of Langmuir model [41]. This describes the participation of chemisorption mechanism in the adsorption process of MB on CC. The validity of Langmuir model can also be proved through a dimensionless constant, called equilibrium parameter R_L (separation factor, Eq. (6)) [42], which measures the suitability of CC as an adsorbent for removal of the MB dye:

$$R_L = \frac{1}{1 + K_L C_0} \quad (6)$$

Adsorption of any pollutant is regarded favorable, if R_L value follows $0 < R_L < 1$, whereas unfavorable ($R_L > 1$), linear ($R_L = 1$), and irreversible ($R_L = 0$). In present study, R_L value for CC is 0.150, which displays the favorability of the studied adsorbent for MB dye adsorption. This also indicates the formation of monolayer of adsorbate molecules onto the homogeneous surface of the CC adsorbent. Similarly, adsorption of MB onto citrus fruit peel has also been best described by Langmuir model [43].

3.4.2. Freundlich isotherm

Freundlich isotherm (Eq. (7)) considers the heterogeneous surface of the adsorbent:

$$q_e = K_F C_e^{1/n} \quad (7)$$

The relative adsorption capacity (K_F) and the heterogeneity factor ($1/n$) were calculated from the plot, q_e vs. C_e i.e. (17.17 L g⁻¹) and 0.419 (Table 1), which

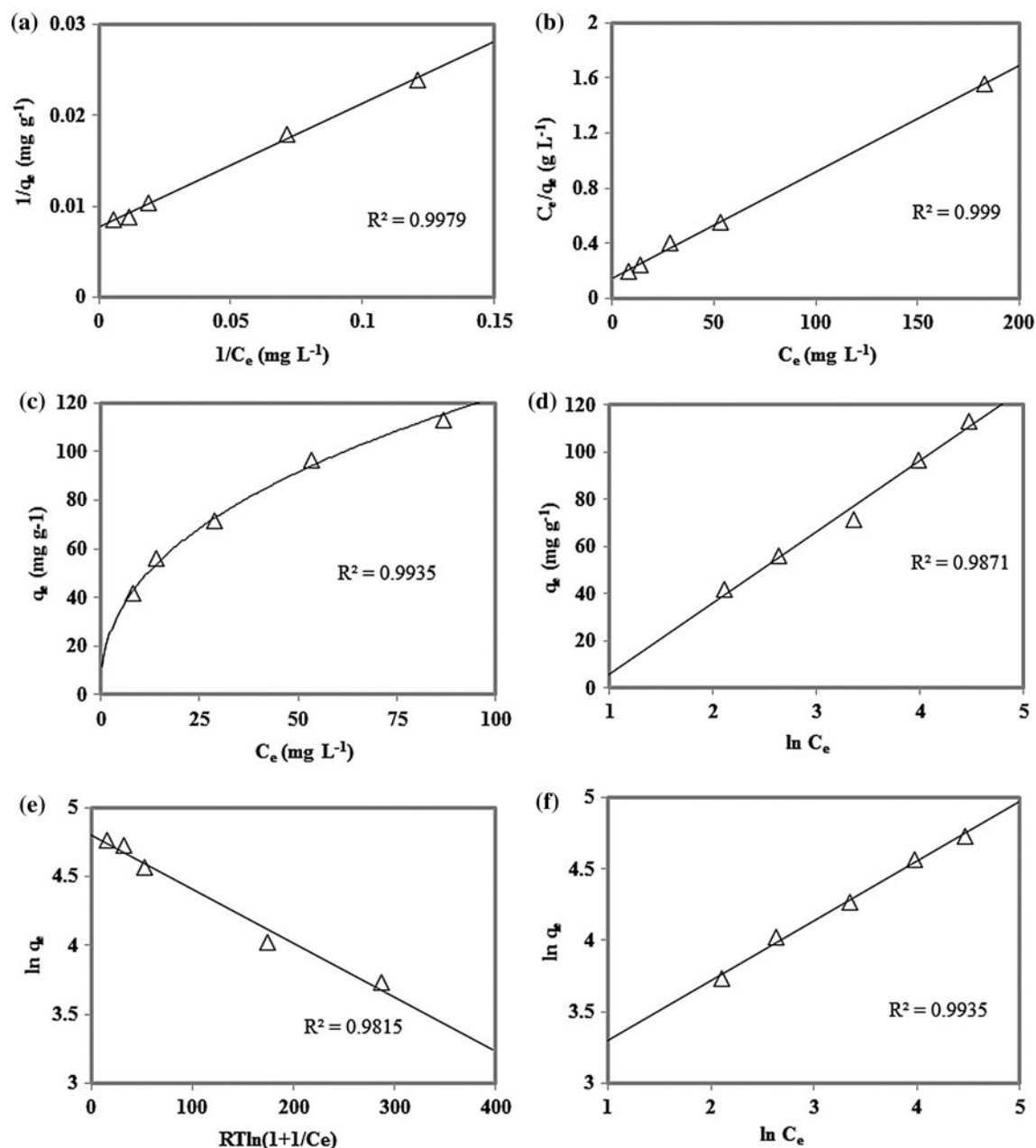


Fig. 6. Isotherm model plots (a) Langmuir 1, (b) Langmuir 2, (c) Freundlich, (d) Tempkin, (e) D-R, (f) Halsey. Initial dye concentration range = 50–300 mg L⁻¹, $m = 1$ g L⁻¹ for $t = 200$ min at 220 rpm and 303 K.

indicated the intensity and feasibility of the adsorption process, respectively. The value of $1/n$ (Freundlich exponent) should be less than 1 for the favorable adsorption [38,44,45]. This confirmed the usefulness of CC adsorbent for MB adsorption from the aqueous solution. Coefficient of determination (R^2) was 0.9935, which showed a better fit to the equilibrium data than the other models, however, lesser fit than Langmuir model (Fig. 6). This further revealed the dominance of active sites with homogeneous energy distribution.

3.4.3. Halsey isotherm

This model is suitable for multilayer adsorption (Eq. (8)):

$$\ln q_e = \frac{1}{n_H} \ln K_H - \frac{1}{n_H} \ln C_e \quad (8)$$

where K_H and n_H are Halsey's isotherm constants, which were obtained from the slope and intercept of

the plot $\ln C_e$ vs. $\ln q_e$. Equilibrium data showed a good fit to this model with R^2 , 0.9935 (Fig. 6), which confirmed the heterogeneous pore distribution. The R^2 value and closeness of q_{cal} (115 mg g⁻¹) predicted by Halsey model with that of q_{exp} (117 mg g⁻¹) validate the hypothesis of Freundlich model.

3.4.4. Temkin isotherm

This isotherm model hypothesized that heat of adsorption of all the molecules in the layer decreases linearly rather than logarithmic during the course of adsorption [46]. The adsorption process is characterized by equal distribution of binding energies at the adsorbent surface up to some maximum binding energy [40,47]:

$$q_e = \frac{RT}{B} \ln(A_T C_e) \quad (9)$$

$$B = \frac{RT}{b} \quad (10)$$

In Eqs. (9) and (10), A_T (L g⁻¹) is the equilibrium binding constant; B (kJ mol⁻¹) is the rate constant related to adsorption energy; T and R are absolute temperature (K) and universal gas constant (8.314 J mol⁻¹ K⁻¹). The constants A_T and b_T were calculated from the plot q_e vs. $\ln C_e$. Temkin model indicated the good fit to the adsorption data with R^2 value of 0.9871 (Fig. 6, and Table 1).

3.4.5. D–R isotherm

The physisorption or chemisorption nature of the interaction between adsorbate and adsorbent were investigated by D–R isotherm [48]. D–R model is given in Eq. (11).

$$\ln q_e = \ln q_{DR} - \beta \varepsilon^2 \quad (11)$$

where q_{DR} is the theoretical monolayer sorption capacity (mg g⁻¹) and β is the constant of adsorption energy (mol² K J⁻²). Whereas ε is the Polanyi potential, which is calculated by Eq. (12):

$$\varepsilon = RT \quad (12)$$

where T and R are the temperature and universal gas constant (8.314 J mol⁻¹ K⁻¹), respectively. It is observed from Fig. 6 that the R^2 value (0.9815) is lower than that of Langmuir, Freundlich, Halsey and

Temkin isotherm models. Theoretical monolayer sorption capacity (q_{DR} , 122.13 mg g⁻¹) calculated by D–R model was in close agreement with q_{exp} (117 mg g⁻¹), which reflect the applicability of this model for the accurate prediction of equilibrium results. Constant of adsorption energy (β , mol² J⁻²) was calculated as 0.0019 mol² J⁻². Data also showed the value of mean free energy (16.01 kJ mol⁻¹) (Eq. (11), Table 1), which means that one mole of adsorbate will require 16.01 kJ mol⁻¹ to reach the active adsorption sites from an infinite distance.

$$E = \frac{1}{\sqrt{-2\beta}} \quad (13)$$

It depicts the chemisorption nature of adsorbate and adsorbent interaction at solid solution interface with the involvement of ion-exchange mechanism, i.e. 8–16 kJ mol⁻¹ [49]. Based on the coefficient of determination (R^2), isotherm models fit to the equilibrium adsorption data and exhibit the following order Langmuir > Freundlich > Halsey > Temkin > D–R (Table 1, Fig. 6). Although, the adsorption of MB on CC was mainly controlled by chemisorption as confirmed through regression coefficients Langmuir and E value of D–R model, yet the high correlation coefficients, for rest of the applied isotherm models were also suggested the involvement of the physisorption process at low coverage, i.e. R^2 values of Freundlich and Halsey (0.9935). Therefore, there is a possibility of multilayer adsorption of MB dye onto the surface of CC and data fitness to Halsey model attests that multilayer adsorption is present at larger distance from the adsorbent surface.

3.5. Thermodynamic study

Thermodynamic parameters were determined to assess the effect of temperature on CC biosorbent for MB adsorption (Table 3).

The distribution coefficient K_d was calculated from Eq. (14):

$$K_d = \frac{q_e}{C_e} \quad (14)$$

where q_e is the solid phase concentration and C_e is the liquid phase concentration at equilibrium. This was further used in Van't Hoff plot. Change in enthalpy and entropy were calculated from Van't Hoff plot using Eq. (15):

$$\ln K_d = \frac{\Delta S}{R} - \frac{\Delta H}{RT} \quad (15)$$

where ΔH (kJ mol^{-1}) is the change in standard enthalpy, ΔS is a change in standard entropy (kJ mol^{-1}), R is universal gas constant ($8.314 \text{ J mol}^{-1} \text{ K}^{-1}$), and T is the temperature (K). The values of $\Delta H > 0$ and $\Delta S > 0$ were calculated as 48 kJ mol^{-1} and $170 \text{ J mol}^{-1} \text{ K}^{-1}$, respectively. This demonstrates that the reaction is endothermic in nature and adsorption of MB dye increases with an increase in temperature. However, an increase in randomness is observed at the solid–liquid interface, which reflects some structural changes on the surface of adsorbent with increasing temperature. ΔG (Gibbs free energy change, kJ mol^{-1}) values were obtained from the Eq. (16):

$$\Delta G = \Delta H - T\Delta S \quad (16)$$

The values of ΔG were found to be -3.37 , -4.24 , -5.10 , -5.96 , $-6.82 \text{ kJ mol}^{-1}$, respectively, at 303, 308, 313, 318, and 323 K temperatures. Negative values of ΔG confirmed that the adsorption of MB onto CC was a (an exergonic) spontaneous reaction at any temperature. This implies that the adsorption system does not require an external energy source. The results from thermodynamic study are in good agreement with experimental data (Fig. 5) as the increasing temperature is equally effective for high biosorption capacity and removal percentage of MB dye.

3.6. Adsorption kinetics

The rate-limiting step was investigated using the pseudo-first-order and pseudo-second-order reaction models for MB dye adsorption onto CC. Lagergren first-order rate equation (Eq. (17)) is the earliest known one to describe the adsorption rate based on the adsorption capacity:

$$\log(q_e - q_t) = \log q_e - \frac{K_1 t}{2.303} \quad (17)$$

whereas q_t (mg g^{-1}) is the amount of adsorbate adsorbed at time t and K_1 (min^{-1}) is the pseudo-first-order rate constant. The driving force, $(q_e - q_t)$, is proportional to the available fraction of active sites. Values of the rate constant (K_1 , 0.009–0.015), equilibrium adsorption capacity (q_e , 9–78 mg g^{-1}), and the correlation coefficients (R^2 , 0.438–0.876) were calculated from $\log(q_e - q_t)$ vs. t plot (Table 2). CC did not reflect a strong correlation in the most cases, which indicated that the film diffusion or mass transfer property is not the primary rate-controlling process

[50]. Moreover, differences between experimental q_e and calculated q_{cal} indicated that the adsorption kinetics of the pseudo-first-order model could not be reproduced.

The pseudo-second-order model equation is given in Eq. (18).

$$\frac{t}{q_t} = \frac{1}{K_2 q_e^2} + \frac{1}{q_e} t \quad (18)$$

where K_2 ($\text{g mg}^{-1} \text{ min}^{-1}$) is the pseudo-second-order rate constant and h ($\text{mg g}^{-1} \text{ min}^{-1}$) is the initial adsorption rate, which is a complex function of the solute concentration [50]. Initial adsorption rate ($h = K_2 q_e^2$) and rate constant (K_2), were determined from the intercept and the slope of the plot t/q_t vs. t . The R^2 values (0.947–0.992) (Fig. 7) indicated that the adsorption of MB dye onto CC obeyed the pseudo-second-order model in contrast to pseudo-first-order kinetic model. This suggests that the rate-limiting step may be the chemisorption involving valence forces through sharing or exchange of electrons between the adsorbent and adsorbate. Moreover, a good agreement was observed between the calculated ($q_{e,\text{cal}}$) values with that of experimental $q_{e,\text{exp}}$ values (Table 2). However, the coefficient of determination decreased with the increasing MB dye (solute) concentration. This means that MB adsorption follows the second-order rate law, and affirms the dye adsorption is related to the availability of adsorption sites rather than dye concentration in the aqueous solution. Moreover, it also suggests the quicker MB dye adsorption rate at lower dye concentration and vice versa, under the same experimental conditions. This model has also been reported to well describe the adsorption of metal ions, dyes, herbicides, oils, and organic substances from aqueous solutions [45,51].

3.7. Desorption studies

Desorption of MB dye from the CC adsorbent was obtained as 78.8, 78.1, 72.1, 56.96, and 56.7%, respectively, by various eluents, i.e. 0.1 M acetic acid (AA), sulfuric acid (SA), hydrochloric acid (HA), and NA, respectively (Fig. 8). Whereas by solvents like methanol (Mt), ethanol (Et), and acetone (At), desorption of MB was found to be 56.9, 51.1, and 42.9%, respectively. The higher recovery percentage of MB with acids can be attributed to the involvement of ions exchange and chemisorption as binding mechanisms between the adsorbent and adsorbate.

Table 2
Constants calculations of kinetic models

| Initial MB dye Conc. (mg L ⁻¹) | Pseudo-first-order | | | | Pseudo-second-order | | | |
|---|--------------------------------------|-------------------------------|--------------------------------------|-------|--|--------------------------------------|--|-------|
| | $q_{e,exp}$ (mg g ⁻¹) | K_1 (min ⁻¹) | $q_{e,cal}$ (mg g ⁻¹) | R^2 | K_2 (g mg ⁻¹ min ⁻¹) | $q_{e,cal}$ (mg g ⁻¹) | h (mg g ⁻¹ min ⁻¹) | R^2 |
| 30 | 18.73 | 0.009 | 6.7608 | 0.644 | 0.0061 | 24.7 | 2.145 | 0.990 |
| 50 | 41.73 | 0.018 | 30.90 | 0.847 | 0.0009 | 41.79 | 1.675 | 0.992 |
| 70 | 56.07 | 0.002 | 37.58 | 0.86 | 0.0006 | 58.77 | 2.090 | 0.975 |
| 100 | 71.38 | 0.003 | 54.95 | 0.861 | 0.00028 | 85.98 | 1.430 | 0.947 |

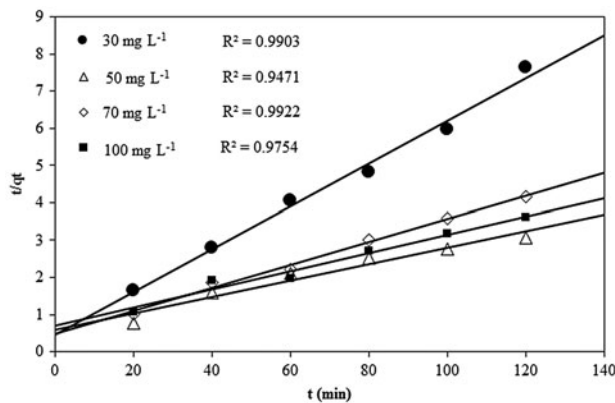


Fig. 7. Pseudo-second-order kinetics model for MB adsorption onto CC at various initial concentrations of MB, i.e. 30, 50, 70, and 100 mg L⁻¹.

3.8. Column studies

Continuous biosorption experiments in a fixed-bed column were conducted in a glass column (50 cm height), packed with corncob biomass. At the bottom of the column, 3 mm glass beads were attached followed by a layer of glass wool. A known quantity of the CC was packed in the column to yield the desired bed height of the biosorbent (5–10 cm). The MB solution of known concentrations (50, 150, and 300 mg L⁻¹) at pH 7 was pumped in upward of the column at a desired flow rate (5, 7, and 10 mL min⁻¹) regulated by a peristaltic pump. The dye solutions at the outlet of the column were collected at regular time intervals, and the concentration was measured using a double beam UV-vis spectrophotometer (PG instruments T80⁺, UK) at 668 nm. All the experiments were carried out at room temperature. Effluent volume (V_{eff}) can be calculated from Eq. (19) as:

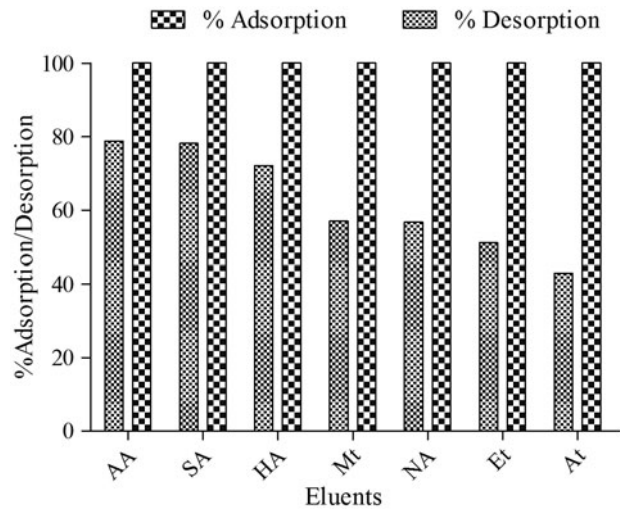


Fig. 8. Desorption of MB dye from CC after treating with various eluents at 0.1 M concentrations, i.e. AA, SA, HA, Mt, Et, At.

$$V_{eff} = F \times t_{total} \quad (19)$$

where t_{total} and F are the total flow time (min) and volumetric flow rate (mL min⁻¹). Breakthrough capacity $Q_{0.5}$ (at 50% or $C_t/C_0 = 0.5$) expressed in mg of dye adsorbed per gram of adsorbent (mg g⁻¹) and it was calculated by the following equation:

$$\text{Breakthrough capacity } (Q_{0.5}) = \frac{\text{dye adsorbed on biosorbent bed (mg)}}{\text{mass of adsorbent in the bed (g)}} \quad (20)$$

$$Q_{0.5} = \frac{(\text{breakthrough time at (50\%)} \times \text{flow rate} \times \text{inlet concentration})}{\text{mass of biosorbent in the bed (g)}} \quad (21)$$

3.8.1. Effect of initial dye concentration

The effect of the various inlet concentration of MB from 50 to 300 mg L⁻¹ was assessed by taking the fixed-bed height of 5 cm and solution flow rate of 5 mL min⁻¹. It is illustrated in Fig. 9 that the breakthrough time is decreased with increasing concentrations of MB influent. At low influent MB concentrations, breakthrough were dispersed and breakthrough occurred slowly as the influent concentration increased. These results demonstrated the fact that a lower concentration gradient caused a slower transport due to a decrease in the diffusion coefficient or mass transfer coefficient. The higher inlet concentration, the steeper is the slope of the breakthrough curve and smaller is the breakthrough time. These results demonstrate that the change of the concentration gradient affects the saturation rate and breakthrough time, or in other words, the diffusion process is concentration-dependent. An increase in the dye concentration increases the MB loading rate, which is the driving force for mass transfer, which decreases the adsorption zone length. Similar trends have been

obtained for biosorption of MB by chitosan-clay composite [52] and rice husk [53]. The adsorption capacity was expected to increase with increasing the inlet concentration because a high concentration difference provides a high driving force for the adsorption process. The highest bed capacity of 94 mg g⁻¹ was obtained using 300 mg L⁻¹ inlet MB concentration, 5 cm bed height, and 5 mL min⁻¹ flow rate.

3.8.2. Effect of corncob bed height

Fig. 9 showed the breakthrough curve for different bed heights of 5, 7, and 10 cm (5.7, 8.6, and 11.5 g), at a constant flow rate of 5 mL min⁻¹ of influent MB dye concentration of 50 mg L⁻¹. It is also evident that both the breakthrough and break time increased with increasing the bed height (Fig. 9). MB dye had more time to contact with CC with increasing bed height that was resulted in high sorption efficiency of biosorbent for dye. Therefore, the column with high bed height showed a decrease in the effluent solute concentration at the same time. The results also indicated

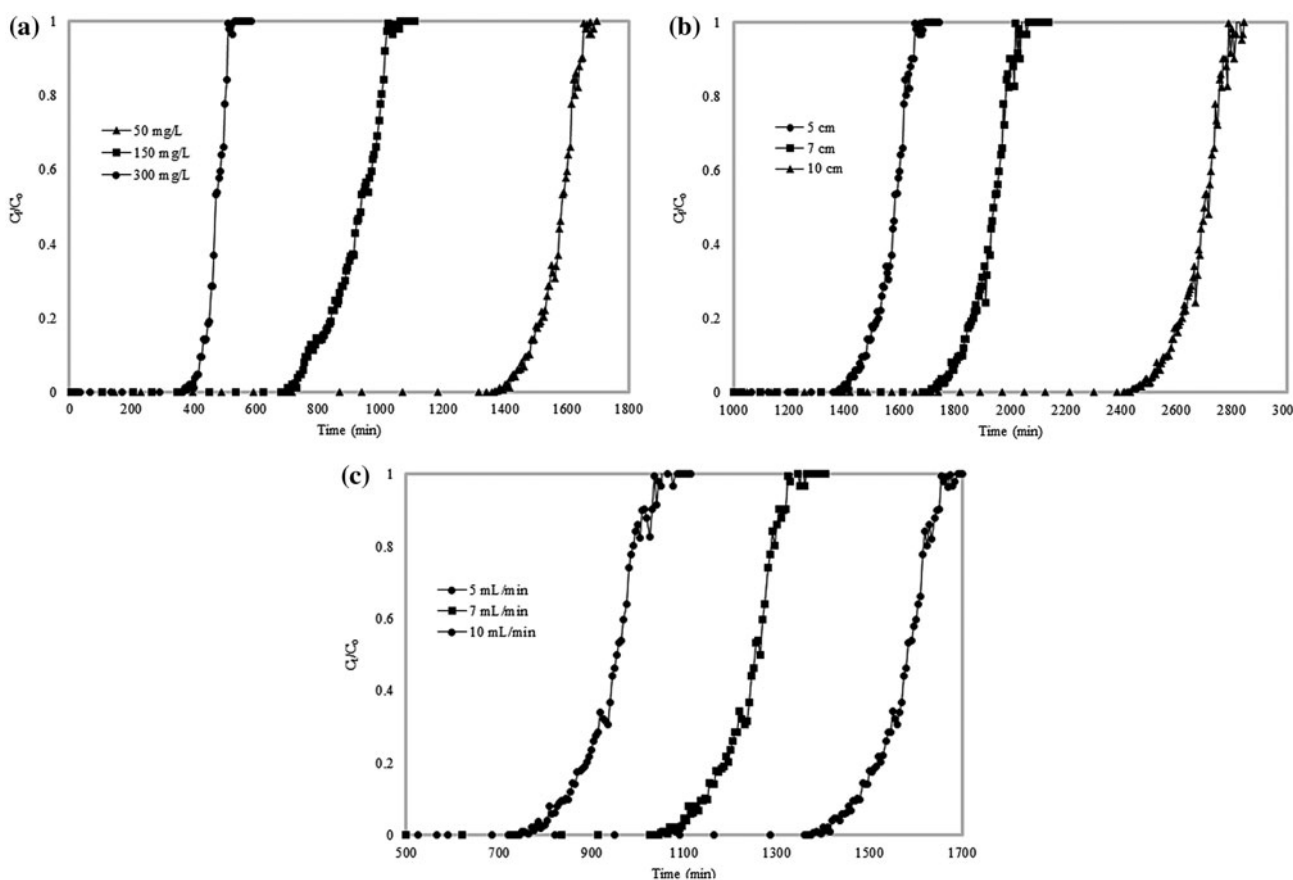


Fig. 9. Breakthrough curves at variable initial (a) dye concentration, (b) bed height, and (c) flow rate.

the increased total solution volume at high bed height, due to the availability of more sorption sites. This shows that the effluent/influent adsorbate concentration ratio increased more rapidly at smaller bed height than that at higher bed height. Furthermore, saturated zone is established in lesser time at smaller bed height and vice versa.

3.8.3. Effect of the solution flow rate

The effect of the influent flow rate on the adsorption of MB using the CC was investigated by varying the flow rate (5, 7, and 10 mL min⁻¹) with a constant adsorbent bed height of 5 cm and the inlet MB concentration of 50 mg L⁻¹, as shown by the breakthrough curve in Fig. 9. It was shown that breakthrough generally occurred faster with higher flow rate. At low flow rate inlet MB, the breakthrough time reaching saturation was considerably increased. Because the inlet MB dye had more time to contact with adsorbent, in turn, it resulted in high removal of MB dye. The variations in the breakthrough curve slope and sorption capacity can be described on mass transfer fundamentals. The rate of mass transfer increases at a high flow rate, i.e. the amount of MB adsorbed per unit bed height/mass transfer zone increased and ultimately leading to fast saturation. Moreover, the adsorption capacity was diminished due to insufficient residence time in the column, and interparticle pore diffusion of the solute. Therefore, the solute left the column prior to the establishment of equilibrium. Similar observations have been reported in the literature [54].

3.9. Modeling of fixed-bed column breakthrough

The kinetics and mass transfer models have been established to predict the dynamic behavior of the column. These models have been used effectively to determine the breakthrough performance, kinetic parameters, and adsorption capacity of the fixed-bed

column. The models include Thomas, and bed depth service time (BDST).

3.9.1. Thomas model

Thomas model is one of the most commonly used kinetic model in the column performance operations. This model assumes that the adsorption process follows Langmuir isotherm of adsorption–desorption with no axial dispersion, and the driving force is the second-order reversible reaction kinetics. It also takes into account the application of a separation factor to estimate the favorable or unfavorable adsorption isotherm.

The column data were fitted to the Thomas model to determine the Thomas rate constant (K_{th}) and maximum solid-phase concentration (q_0) (Eq. (22)):

$$\ln\left(\frac{C_0}{C_t} - 1\right) = \frac{K_{th} q_0 W}{Q} - K_{th} C_0 t \quad (22)$$

where K_{th} (mL min⁻¹ mg⁻¹) is the Thomas rate constant; q_0 (mg g⁻¹) is the equilibrium MB uptake per g of the biosorbent; C_0 (mg L⁻¹) is the inlet dye concentration; C_t (mg L⁻¹) is the outlet concentration at time t ; W (g) the mass of adsorbent, Q (mL min⁻¹) the flow rate, and t total (min) stands for flow time. The coefficients of correlation and relative constants were obtained using linear regression analysis (Eq. (22)). The results demonstrated an increase in q_0 with the increase in dye concentration but decreased with increasing flow rate. An opposite trend was observed for K_{th} values which were determined by Thomas model (Table 3 and Fig. 10).

3.9.2. BDST model

The model predicts the linearity between the bed depth X and service time t (Eq. (23)). This model suggests that the forces like intra-particle diffusion and

Table 3
Thomas model parameters at different conditions using linear regressions analysis

| Inlet concentration (mg L ⁻¹) | CC bed height (cm) | Flow rate (mL min ⁻¹) | K_{th} (mL min ⁻¹ mg ⁻¹) | q_0 (mg g ⁻¹) | R^2 |
|---|--------------------|-----------------------------------|---|-----------------------------|-------|
| 50 | 5 | 5 | 0.468 | 52.05 | 0.971 |
| 50 | 5 | 7 | 0.572 | 57.45 | 0.88 |
| 50 | 5 | 10 | 0.672 | 62.43 | 0.92 |
| 50 | 7 | 5 | 0.540 | 49.49 | 0.914 |
| 50 | 10 | 5 | 0.426 | 44.58 | 0.922 |
| 150 | 5 | 5 | 0.117 | 93.43 | 0.914 |
| 300 | 5 | 5 | 0.165 | 94.78 | 0.972 |

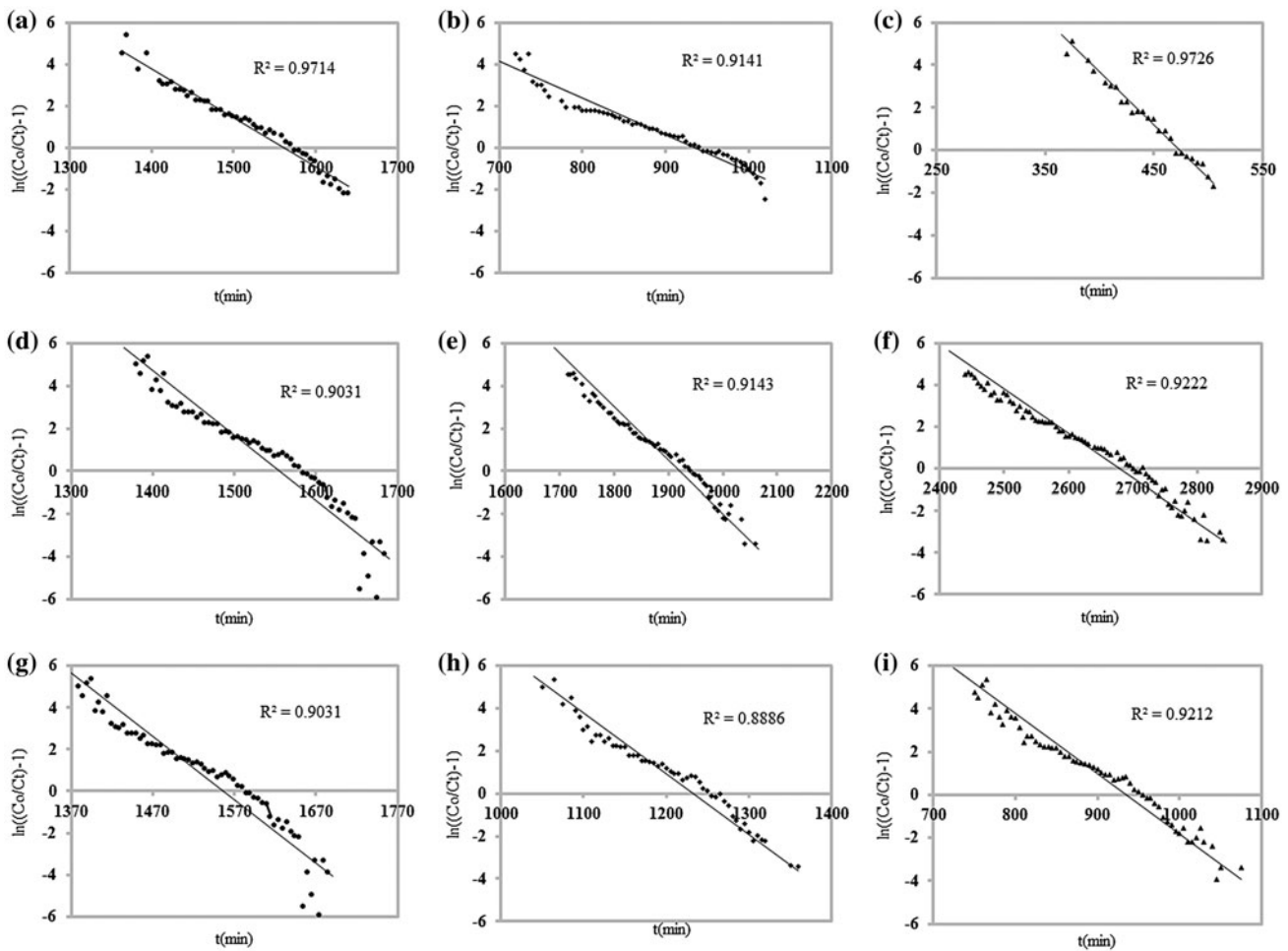


Fig. 10. Thomas model application (a) 50 mg L⁻¹, (b) 150 mg L⁻¹, (c) 300 mg L⁻¹, bed height, (d) 5 cm, (e) 7 cm, (f) 10 cm, and flow rate (g) 5 mL min⁻¹, (h) 7 mL min⁻¹, (i) 10 mL min⁻¹.

external mass transfer resistance are negligible and adsorbate is directly adsorbed onto the adsorbent surface. The BDST model can also describe the initial part of the breakthrough curve, i.e. up to break point or 10–50% of saturation points. Moreover, this model focuses on the characteristics parameters such as adsorption capacity and kinetic constants:

$$t = \frac{N_0 Z}{C_0 U} - \frac{1}{K_a C_0} \ln\left(\frac{C_0}{C_b - 1}\right) \quad (23)$$

where C_0 is the initial dye concentration (mg L⁻¹), C_b is the breakthrough dye concentration (mg L⁻¹), U is the linear velocity (cm min⁻¹), N_0 is the adsorption capacity of the bed (mg g⁻¹), K_a is the rate constant in BDST model (L mg⁻¹ min⁻¹), t is the time (min), and Z is the bed height (cm) of the column. The value of K_a shows the rate of transfer from the liquid to the solid phase. When K_a is large even a short bed height, it

will avoid breakthrough but as K_a decreases, a deeper bed is required to avoid breakthrough. The advantage of the BDST model is that any experimental test can be reliably scaled up to other flow rates without further experimental runs.

At 50% breakthrough $C_0/C_t = 2/1$ at $t = t_{0.5}$ the equation is reduced to Eq. (24):

$$t^{0.5} = \frac{N_0 Z}{C_0 U} \quad (24)$$

Analysis of adsorption data by BDST generated the following linear relationship $0.5 = 225.9H + 426.5$ ($R^2 = 0.994$). The model predicts a linear relationship with fairly good regression coefficient but the line does not pass through the origin. Such kind of deviation is caused by more than one rate-limiting step in the adsorption process [55,56]. The slope of

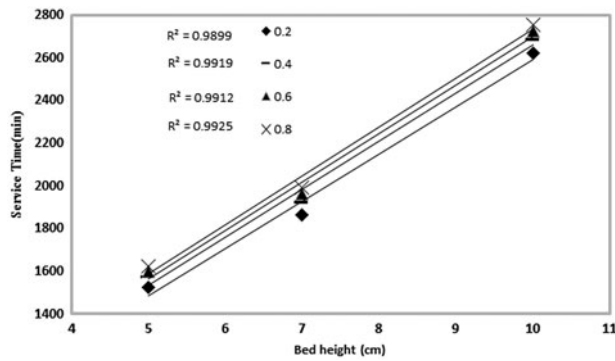


Fig. 11. BDST for CC and MB C_t/C_0 in various bed depths of 5 mL min^{-1} flow rate.

Table 4
BDST model calculations

| C_t/C_0 | A | B | N_0 (mg L^{-1}) | K_a | R^2 |
|-----------|-------|-------|------------------------------|-----------------------|-------|
| 0.2 | 221.5 | 378.4 | 2,819.091 | $-7.32714\text{E-}05$ | 0.989 |
| 0.4 | 225.4 | 408 | 2,868.727 | $-1.98757\text{E-}05$ | 0.991 |
| 0.6 | 227.3 | 427.6 | 2,892.909 | $1.89647\text{E-}05$ | 0.991 |
| 0.8 | 228.2 | 449.2 | 2,904.364 | $6.17228\text{E-}05$ | 0.992 |

225.9 min m^{-1} (Fig. 11) indicates that about 2.26 min are required to exhaust 1 cm of adsorbent.

Among the BDST and Thomas model, the values of correlation coefficients (R^2) as listed in Tables 3 and 4 both provide good fit to column adsorption data at various conditions. In comparison to R^2 values and breakthrough curves, both BDST and Thomas models can be used to describe biosorption behavior of MB on the fixed-bed column. Similar observations were reported by adsorption of MB on *Pisidium guajava* leaf powder [57] and adsorption of direct yellow 50 on sugarcane bagasse [54]. In view of the bulk availability of the corncob (millions tones per year) in Pakistan [58], the process may be recommended for the real applications in treating wastewaters containing MB.

The availability of corn cobs can be estimated as:

$$R_{\text{cob}} = \text{Grain yield} \times \text{CGR} \times \text{Removal\%} \times [1 - \text{Moisture\%}] \quad (25)$$

where R_{cob} is the quantity of harvestable corn cobs in dry ton per acre. Grain yield (Av.yield of grain crop in tons per acre) = 3.5 metric tonnes per hectare = 1.42 tonnes per hectare. CGR is cob-to-grain ratio = 1:5.6 based on [59]. Removal% is percent of cobs that can be removed from farm fields each year = 1. Moisture%

is the moisture content of corn cob = 20%. R_{cob} is 0.2 ton per acre of corn cob. Since total area under maize production is 1 million hectare, therefore:

$$\begin{aligned} \text{Total CC production in KPK} &= 0.2 \text{ tonnes/acre} \times 2.47105 \text{ acre/hectare} \\ &\times 10^6 \text{ hectare} \\ &= 0.5 \times 10^6 \end{aligned} \quad (26)$$

Considering for corncob, $q_e = 50 \text{ mg g}^{-1}$ and if dye concentration is 10 mg L^{-1} , then:

$$\begin{aligned} \text{Adsorbent usage rate} &= \frac{C_0}{q_e} = \frac{10 \text{ mg/L}}{50 \text{ mg/g}} \\ &= 0.2 \text{ g adsorbent/L} \end{aligned} \quad (27)$$

$$\begin{aligned} \text{Textile wastewater that can be treated} &= \frac{\text{total corncob production}}{\text{adsorbent usage rate}} = \frac{5 \times 10^{11}}{0.2} \\ &= 25000 \text{ million m}^3 \end{aligned} \quad (28)$$

Hence, roughly speaking about 25,000 million cubic meter of wastewater containing MB dye can be treated in real situation using corncob as adsorbent.

4. Conclusions

This study shows that the CC biomass depicted efficient biosorption potential for MB dye. The maximum biosorption capacity of CC for MB was found to be 117 mg g^{-1} . Thermodynamic studies suggested the favorable and spontaneous nature of the biosorption reaction at increasing temperature. The batch adsorption data were analyzed by Langmuir, Freundlich, Halsey, Temkin, and D–R the isotherm models. Isotherm models suggest chemisorption mechanism was involved in the biosorption process. The batch adsorption kinetics represent quicker dye adsorption at lower initial dye concentration. The BDST model represents best fits to the adsorption data than Thomas model. High efficiency, low-cost, and reusability of corncob affirm the good choice of corncob biosorbent for MB dye adsorption from waste stream.

Acknowledgments

This work was supported by Higher Education Commission, Pakistan [Project number 20-1915/R&D/10₅₇₅₃]

References

- [1] A. Mittal, Retrospection of Bhopal gas tragedy, *Toxicol. Environ. Chem.* (2015) 1–5, doi: [10.1080/02772248.2015.1125903](https://doi.org/10.1080/02772248.2015.1125903).
- [2] M.M. Ayad, A.A. El-Nasr, Adsorption of cationic dye (methylene blue) from water using polyaniline nanotubes base, *J. Phys. Chem. C* 114 (2010) 14377–14383.
- [3] A. Mittal, R. Ahmad, I. Hasan, Poly (methyl methacrylate)-grafted alginate/Fe₃O₄ nanocomposite: Synthesis and its application for the removal of heavy metal ions, *Desalin. Water Treat.* (2015) 1–14, doi: [10.1080/19443994.2015.1104726](https://doi.org/10.1080/19443994.2015.1104726).
- [4] A. Mittal, R. Ahmad, I. Hasan, Biosorption of Pb²⁺, Ni²⁺ and Cu²⁺ ions from aqueous solutions by L-cysteine-modified montmorillonite-immobilized alginate nanocomposite, *Desalin. Water Treat.* (2015) 1–18, doi: [10.1080/19443994.2015.1086900](https://doi.org/10.1080/19443994.2015.1086900).
- [5] M. Naushad, A. Mittal, M. Rathore, V. Gupta, Ion-exchange kinetic studies for Cd(II), Co(II), Cu(II), and Pb (II) metal ions over a composite cation exchanger, *Desalin. Water Treat.* 54 (2015) 2883–2890.
- [6] A. Mittal, M. Naushad, G. Sharma, Z. AlOthman, S. Wabaidur, M. Alam, Fabrication of MWCNTs/ThO₂ nanocomposite and its adsorption behavior for the removal of Pb(II) metal from aqueous medium, *Desalin. Water Treat.* (2015) 1–7, doi: [10.1080/19443994.2015.1125805](https://doi.org/10.1080/19443994.2015.1125805).
- [7] T. Akar, A.S. Ozcan, S. Tunali, A. Ozcan, Biosorption of a textile dye (Acid Blue 40) by cone biomass of *Thuja orientalis*: Estimation of equilibrium, thermodynamic and kinetic parameters, *Bioresour. Technol.* 99 (2008) 3057–3065.
- [8] V. Gupta, A. Mittal, L. Krishnan, J. Mittal, Adsorption treatment and recovery of the hazardous dye, Brilliant Blue FCF, over bottom ash and de-oiled soya, *J. Colloid Interface Sci.* 293 (2006) 16–26.
- [9] A. Mittal, Adsorption kinetics of removal of a toxic dye, Malachite Green, from wastewater by using hen feathers, *J. Hazard. Mater.* 133 (2006) 196–202.
- [10] A. Mittal, Use of hen feathers as potential adsorbent for the removal of a hazardous dye, Brilliant Blue FCF, from wastewater, *J. Hazard. Mater.* 128 (2006) 233–239.
- [11] Q. Sun, L. Yang, The adsorption of basic dyes from aqueous solution on modified peat-resin particle, *Water Res.* 37 (2003) 1535–1544.
- [12] R. Han, Y. Wang, W. Yu, W. Zou, J. Shi, H. Liu, Biosorption of methylene blue from aqueous solution by rice husk in a fixed-bed column, *J. Hazard. Mater.* 141 (2007) 713–718.
- [13] A. Srinivasan, T. Viraraghavan, Decolorization of dye wastewaters by biosorbents: A review, *J. Environ. Manage.* 91 (2010) 1915–1929.
- [14] J. Mittal, V. Thakur, A. Mittal, Batch removal of hazardous azo dye Bismark Brown R using waste material hen feather, *Ecol. Eng.* 60 (2013) 249–253.
- [15] G. Sharma, M. Naushad, D. Pathania, A. Mittal, G. El-desoky, Modification of *Hibiscus cannabinus* fiber by graft copolymerization: Application for dye removal, *Desalin. Water Treat.* 54 (2015) 3114–3121.
- [16] A. Mittal, J. Mittal, Hen feather: A remarkable adsorbent for dye removal, *Research Trends and Applications, Green Chemistry for Dyes Removal from Wastewater*, Scrivener Publishing LLC, Hoboken, NJ, 2015, pp. 409–457, (ISBN: 978-1-118-72099-8).
- [17] M. Bilal, J.A. Shah, T. Ashfaq, S.M.H. Gardazi, A.A. Tahir, A. Pervez, H. Haroon, Q. Mahmood, Waste biomass adsorbents for copper removal from industrial wastewater—A review, *J. Hazard. Mater.* 263 (2013) 322–333.
- [18] H. Daraei, A. Mittal, M. Noorisepehr, J. Mittal, Separation of chromium from water samples using eggshell powder as a low-cost sorbent: Kinetic and thermodynamic studies, *Desalin. Water Treat.* 53 (2015) 214–220.
- [19] M. Aurangzeb, S. Nigar, M.K. Shah, Benefit cost analysis of the maize crop under mechanized and traditional farming systems in the NWFP, *Sarhad J. Agric.* 23 (2007) 169–176.
- [20] W.S. Alencar, E.C. Lima, B. Royer, B.D. dos Santos, T. Calvete, E.A. da Silva, C.N. Alves, Application of aqai stalks as biosorbents for the removal of the dye prion blue MX-R from aqueous solution, *Sep. Sci. Technol.* 47 (2012) 513–526.
- [21] Q. Zhou, W. Gong, Y. Li, S. Chen, D. Yang, C. Bai, X. Liu, N. Xu, Biosorption of Methylene Blue onto spent corncob substrate: Kinetics, equilibrium and thermodynamic studies, *Water Sci. Technol.* 63 (2011) 2775.
- [22] S.H. Hasan, D. Ranjan, M. Talat, Water hyacinth biomass (WHB) for the biosorption of hexavalent chromium: Optimization of process parameters, *BioResources* 5 (2010) 563–575.
- [23] K.G. Bhattacharyya, A. Sharma, Kinetics and thermodynamics of methylene blue adsorption on neem (*Azadirachta indica*) leaf powder, *Dyes Pigm.* 65 (2005) 51–59.
- [24] M.A.A. Zaini, T.Y. Cher, M. Zakaria, M.J. Kamaruddin, S.H. Mohd. Setapar, M.A. Che Yunus, Palm oil mill effluent sludge ash as adsorbent for methylene blue dye removal, *Desalin. Water Treat.* 52 (2014) 3654–3662.
- [25] M.H. Kalavathy, L.R. Miranda, Comparison of copper adsorption from aqueous solution using modified and unmodified *Hevea brasiliensis* saw dust, *Desalination* 255 (2010) 165–174.
- [26] V.C. Srivastava, I.D. Mall, I.M. Mishra, Removal of cadmium(II) and zinc(II) metal ions from binary aqueous solution by rice husk ash, *Colloids Surf. A: Physicochem. Eng. Aspects* 312 (2008) 172–184.
- [27] V.C. Srivastava, I.D. Mall, I.M. Mishra, Characterization of mesoporous rice husk ash (RHA) and adsorption kinetics of metal ions from aqueous solution onto RHA, *J. Hazard. Mater.* 134 (2006) 257–267.
- [28] L.D. Fiorentin, D.E.G. Trigueros, A.N. Módenes, F.R. Espinoza-Quiñones, N.C. Pereira, S.T.D. Barros, O.A.A. Santos, Biosorption of reactive blue 5G dye onto drying orange bagasse in batch system: Kinetic and equilibrium modeling, *Chem. Eng. J.* 163 (2010) 68–77.
- [29] E. Rubín, P. Rodríguez, R. Herrero, M.E. Sastre de Vicente, Biosorption of phenolic compounds by the brown alga *Sargassum muticum*, *J. Chem. Technol. Biotechnol. Chem. Technol.* 81 (2006) 1093–1099.
- [30] J. Gao, D. Kong, Y. Wang, J. Wu, S. Sun, P. Xu, Production of mesoporous activated carbon from tea fruit peel residues and its evaluation of methylene blue removal from aqueous solutions, *BioResources* 8 (2013) 2145–2160.

- [31] K. Shahul Hameed, P. Muthirulan, M. Meenakshi Sundaram, Adsorption of chromotrope dye onto activated carbons obtained from the seeds of various plants: Equilibrium and kinetics studies, Arab. J. Chem. (in press), doi: 10.1016/j.arabjc.2013.07.058.
- [32] L. Yu, Y.-M. Luo, The adsorption mechanism of anionic and cationic dyes by Jerusalem artichoke stalk-based mesoporous activated carbon, J. Environ. Chem. Eng. 2 (2014) 220–229.
- [33] R. Dod, G. Banerjee, S. Saini, Adsorption of methylene blue using green pea peels (*Pisum sativum*): A cost-effective option for dye-based wastewater treatment, Biotechnol. Bioprocess Eng. 17 (2012) 862–874.
- [34] H. Asfour, O. Fadali, M. Nassar, M. El-Geundi, Equilibrium studies on adsorption of basic dyes on hardwood, J. Chem. Technol. Biotechnol. Chem. Technol. 35 (1985) 21–27.
- [35] M.S.U. Rehman, I. Kim, J.-I. Han, Adsorption of methylene blue dye from aqueous solution by sugar extracted spent rice biomass, Carbohydr. Polym. 90 (2012) 1314–1322.
- [36] M. Auta, B. Hameed, Acid modified local clay beads as effective low-cost adsorbent for dynamic adsorption of methylene blue, J. Ind. Eng. Chem. 19 (2013) 1153–1161.
- [37] I. Langmuir, The adsorption of gases on plane surfaces of glass, mica and platinum, J. Am. Chem. Soc. 40 (1918) 1361–1403.
- [38] H.M.F. Freundlich, Over the adsorption in solution, J. Phys. Chem. 57A (1906) 385–471.
- [39] M.M. Dubinin, L.V. Radushkevich, Equation of the characteristic curve of activated charcoal, Proc. Acad. Sci. USSR, Phys. Chem. Sect. 55 (1947) 331–333.
- [40] M. Temkin, V. Pyzhev, Kinetics of the synthesis of ammonia on promoted iron catalysts, Acta Physiochim. USSR 12 (1940) 217–222.
- [41] Y. Safa, H.N. Bhatti, Kinetic and thermodynamic modeling for the removal of Direct Red-31 and Direct Orange-26 dyes from aqueous solutions by rice husk, Desalination 272 (2011) 313–322.
- [42] K.R. Hall, L.C. Eagleton, A. Acrivos, T. Vermeulen, Pore- and solid-diffusion kinetics in fixed-bed adsorption under constant-pattern conditions, Ind. Eng. Chem. Fundam. 5 (1966) 212–223.
- [43] S. Dutta, A. Bhattacharyya, A. Ganguly, S. Gupta, S. Basu, Application of response surface methodology for preparation of low-cost adsorbent from citrus fruit peel and for removal of methylene blue, Desalination 275 (2011) 26–36.
- [44] M. Ahmaruzzaman, S.L. Gayatri, Activated tea waste as a potential low-cost adsorbent for the removal of p-Nitrophenol from wastewater, J. Chem. Eng. Data 55 (2010) 4614–4623.
- [45] B. Hameed, L. Chin, S. Rengaraj, Adsorption of 4-chlorophenol onto activated carbon prepared from rat-sawdust, Desalination 225 (2008) 185–198.
- [46] C. Aharoni, M. Ungarish, Kinetics of activated chemisorption. Part 2—Theoretical models, J. Chem. Soc., Faraday Trans. 1: Phys. Chem. Condensed Phases 73 (1977) 456–464.
- [47] P.S. Kumar, R. Gayathri, Adsorption of Pb²⁺ ions from aqueous solutions onto bael tree leaf powder: Isotherms, kinetics and thermodynamics study, J. Eng. Sci. Technol. 4 (2009) 381–399.
- [48] M. Dubinin, The potential theory of adsorption of gases and vapors for adsorbents with energetically nonuniform surfaces, Chem. Rev. 60 (1960) 235–241.
- [49] K.Y. Foo, B.H. Hameed, Insights into the modeling of adsorption isotherm systems, Chem. Eng. J. 156 (2010) 2–10.
- [50] N.A. Oladoja, C.O. Aboluwoye, Y.B. Oladimeji, A.O. Ashogbon, I.O. Otemuyiwa, Studies on castor seed shell as a sorbent in basic dye contaminated wastewater remediation, Desalination 227 (2008) 190–203.
- [51] Y.S. Ho, T.H. Chiang, Y.M. Hsueh, Removal of basic dye from aqueous solution using tree fern as a biosorbent, Process Biochem. 40 (2005) 119–124.
- [52] M. Auta, B. Hameed, Chitosan–clay composite as highly effective and low-cost adsorbent for batch and fixed-bed adsorption of methylene blue, Chem. Eng. J. 237 (2014) 352–361.
- [53] S.-H. Lin, R.-S. Juang, Y.-H. Wang, Adsorption of acid dye from water onto pristine and acid-activated clays in fixed beds, J. Hazard. Mater. 113 (2004) 195–200.
- [54] S. Sadaf, H.N. Bhatti, S. Nausheen, M. Amin, Application of a novel lignocellulosic biomaterial for the removal of Direct Yellow 50 dye from aqueous solution: Batch and column study, J. Taiwan Inst. Chem. Eng. 47 (2015) 160–170.
- [55] D. Sharma, C. Forster, Column studies into the adsorption of chromium (VI) using sphagnum moss peat, Bioresour. Technol. 52 (1995) 261–267.
- [56] K.-S. Low, C.-K. Lee, B.-F. Tan, Quaternized wood as sorbent for reactive dyes, Appl. Biochem. Biotechnol. 87 (2000) 233–245.
- [57] V. Ponnusami, S. Vikram, S. Srivastava, Guava (*Psidium guajava*) leaf powder: Novel adsorbent for removal of methylene blue from aqueous solutions, J. Hazard. Mater. 152 (2008) 276–286.
- [58] Maize (Corn) Crop in Pakistan. Available from: <<http://edu.par.com.pk/wiki/maize/#area-production-and-yield-of-maize>> (accessed 03 March 2016).
- [59] A. Wiseloge, S. Tyson, D. Johnson, Biomass feedstock resources and composition, in: C.E. Wyman (Ed.), Handbook of Bioethanol: Production and Utilization, Taylor and Francis Press, Washington, DC, 1996.